MIXED CONVECTION ANALYSIS OF NANOFLUID FLOW INSIDE AN INDENTED MICROCHANNEL

Kamel BOUARAOUR [a,*], Djemoui LALMI [a] and Mohamed Salem SIDI MOHAMED [b]

[a] University of Ghardaia. Ghardaia 47000. Algeria

[b] University of Nouakchott Al Aasriya, Faculty of Science and Technology (FST), Department of Physics, Mauritania

* Corresponding author, e-mail: bouaraourk@yahoo.fr

The present investigation employed computational techniques to analyze the heat transfer and fluid flow properties of a Water/Cu nanofluid moving through a rectangular microchannel. The upper wall of the microchannel is thermally insulated, while the lower wall is equipped with a ribbed surface maintained at a greater temperature than the fluid entering the channel. The governing equations were discretized using the finite volume method and solved using the ANSYS-Fluent 16.0 Computational Fluid Dynamics software. The study investigated the influence of many parameters, such as the Reynolds number ($20 \leq Re \leq 200$), volume percentages of nanoparticles ($1\% \leq \varphi \leq 8\%$), and rib height. The numerical results demonstrate that when the height of the ribs rises ($e = 20$, $e = 30$, and $e = 40$ μm), the contact surface area between the ribs and the nanofluid similarly increases. As a result, the friction factor of the heated surface rises, regardless of whether the Reynolds numbers are low or high. Furthermore, numerical analysis suggest that the average friction factor diminishes as the Reynolds number rises for all rib heights. Ribs in the microchannel facilitate improved mixing, resulting in heightened heat transfer. The impact is intensified by augmenting the concentration of nanoparticles and the Reynolds numbers at all rib heights.

Keywords: heat transfer, friction factor, nanoparticles, volume fraction.

1. Introduction

Conventional fluids used for cooling systems and engine components, such as water and air, are not effective in some cases since they have low thermal conductivity. In order to overcome this constraint, different techniques are applied, with one prominent strategy being the utilization of nanofluids, which are recognized for their improved thermal efficiency [1-2].

Preliminary research has confirmed, through both analytical and experimental methods, that microchannels effectively cool high-density electrical devices using water [3]. Microchannels incorporating ribs have demonstrated remarkable cooling efficiency. Akbari et al. [4] investigated the impact of ribs on the flow characteristics of water-aluminum oxide nanofluid and heat transfer in a rectangular microchannel. The study involved manipulating the nanoparticle proportions in the nanofluid under laminar flow conditions. The core region of the ribbed microchannel received uniform heat input from all directions, and simulation results were compared with those of a smooth microchannel with identical geometrical and boundary conditions. The data indicated that higher Reynolds numbers or increased nanoparticle volume fractions result in higher fluid temperatures at the microchannel exit. An

analysis of the Nusselt number and friction factor revealed that higher nanoparticle volume fractions enhance heat transmission and friction factors compared to water, attributed to increased viscosity.

A separate empirical study explored the impact of semi-attached T-shaped spikes on the flow and turbulent heat transfer of silver-water nanofluids in 3D trapezoidal microchannels, considering various nanoparticle concentrations [5]. To ensure the reliability of the findings, results were cross-referenced with existing literature. The study's outcomes hold potential for guiding the development of advanced microchannels for applications in solar panels and electronic devices.

Esfahani and Toghraie [6] conducted an experimental study to assess the thermal conductivity of nanofluids at temperatures ranging from 25 to 50 °C. The nanofluid, comprising Silica and Water-Ethylene glycol, had varying volume fractions (0.1%, 0.5%, 1%, 1.5%, 2%, 3%, and 5%). The investigation revealed a positive correlation between thermal conductivity and both temperature and volume fraction. Notably, the volume fraction had a more substantial impact on thermal conductivity. The study derived an equation to predict the thermal conductivity of the Silica/Water-Ethylene glycol nanofluid, showing a maximum deviation of 2.2%.

A numerical study by Aghanajaf et al. [7] explored distilled water and CuO particles with volume fractions of 1%, 2%, and 4%. The study considered laminar flow with a Reynolds number of 100 and addressed two boundary conditions: constant heat flux on all sides for validation and constant heat flux on two sides with constant temperature on one side (hot plate). The investigation extensively examined convective heat transfer coefficient, Nusselt number, pressure loss within the channel, velocity distribution, and wall temperature. The use of nanofluids resulted in a significant increase in the heat transfer coefficient, with CuO particles contributing to increased pressure loss and influencing velocity distribution. The study demonstrated a strong correlation between the obtained results and experimental data from existing literature.

In their investigation, Arabpour et al. [8] introduced slip boundary conditions and included oscillatory heat flow to the walls of the microchannel. The numerical simulations demonstrate that the friction coefficient shows a declining pattern when the slip velocity increases. Including partial slip boundary conditions in the microchannel improves the precision of the single-phase homogeneous method compared to experimental data [9]. Khodabandeh et al. [10] investigated a new microchannel configuration in which a constant heat flux is delivered to the walls of the microchannel. They conducted experiments at four Reynolds numbers: Re = 50, 300, 700, and 1000. The numerical results demonstrated that the volume percentages of nanoparticles influence the Nusselt number, the geometry of the inlet, and the Reynolds number. The study found that the inclusion of ribs in the microchannel improves mixing. Additionally, when the concentration of nanofluid increases, there is a corresponding increase in both pressure drop and velocity gradients.

A recent numerical investigation examined a nanofluid's laminar flow and heat transfer consisting of water and silver particles. The study focused on Reynolds numbers 150, 300, 500, and 700 [11]. The study's findings are displayed using localized and averaged flow and heat transmission region maps. Significantly, when the Grashof number increases, the dimensionless temperature along the center streamline decreases. The thermal boundary layer gets more distinct after the angle exceeds 30° at a Reynolds number of 500. In places characterized by low Grashof numbers, there is a notable occurrence of entropy formation caused by the significant influence of temperature differences near the wall.

Understanding the arrangement of ribs is crucial for comprehending the fluid flow behavior and heat transfer properties crucial for cooling purposes. Gholami et al. [12] explored the influence of different rib shapes on nanofluid flow and heat transfer in a rectangular microchannel. The study utilized the finite volume approach to conduct simulations at Reynolds numbers of 1, 10, 50, and 100, considering nanoparticle volume fractions of 0, 2, and 4%. Among the various rib shapes investigated, the parabolic rib exhibited the highest proportional increase in the Nusselt number with an accompanying rise in the friction factor. The integration of nanofluids into microchannels provides opportunities for combining with other elements such as magnetic fields [13-14], porous medium [15-17], and non-Newtonian fluids [18-19]. Recent research has established a connection between examining nanoparticles and using artificial intelligence to enhance the efficiency of computational fluid dynamics (CFD) computations [20]. In addition, the study investigates the utilization of various nanoparticles to improve the effectiveness of heat transmission by examining their chemical and physical properties [21-22].

The present study investigates the impact of rib heights of a laminar nanofluid flowing through a rectangular microchannel with indentations. The temperature of the indentation wall is intentionally kept higher than the inlet temperature to create the combined convection regime. This approach differs from the typical practice of considering a regular heat flux, as seen in many previous research studies. This work distinguishes itself from Gravndyan et al.'s research [23] by exclusively examining differences in rib height rather than variations in ribbed pitch. This investigation considers Reynolds numbers ranging from Re = 20 to Re = 200.

2. Problem description

This study examines the movement of a smooth Cu/water nanofluid via a rectangular micro-channel, which is defined by its length (L) and height (H). The inquiry centres on the manipulation of rib heights, specifically with three distinct values: e = 20 μm, e = 30 μm, and e = 40 μm. The width (w) of each rib is 40 μm, and the distance between subsequent ribs is twice the width (2w). The upper wall of the microchannel is thermally isolated, while the bottom wall, from the entrance to the beginning of the ribs, is kept at a constant temperature. A high temperature (θh) is applied from the start of the indented lower surface to the microchannel outlet. A mixed convection is then created inside the microchannel, due to the combination between forced convection caused by inlet velocity and natural convection induced by temperature difference. Figure 1 presents a graphic representation of the analysed setup.

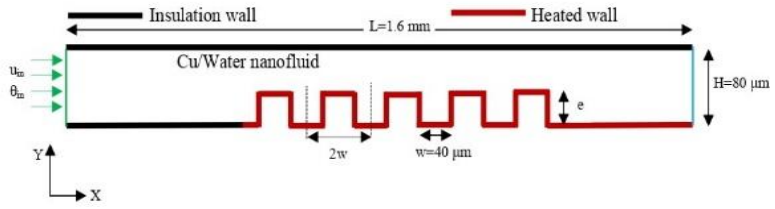

Figure 1. Configuration of the indented microchannel.

The thermophysical properties of Cu nanoparticles and water (Pr = 6.2) as base fluid are listed in Table 1.

Table 1. Thermo-physical properties of water and nanoparticles at T = 300 K (Incropera [24]).

	H_2O	Cu
C_p ($J.Kg^{-1}.K^{-1}$)	4179	385
ρ (Kg/m^3)	997.1	893
k ($W.m^{-1}.K^{-1}$)	0.613	401
μ ($Kg.m^{-1}.s^{-1}$)	0.855x10	-

3. Mathematical formulation

The transmission of heat and flow of nanofluid within the microchannel is regulated by the continuity equation, the Navier-Stokes equations, and the energy equation. The dimensional form of these equations is given by the equations (1)-(3). The flow is characterized as laminar, incompressible, and consisting of a single phase. The solid nanoparticles are in thermal equilibrium with water.

$$\frac{\partial(\rho_{nf}u_i)}{\partial x_i}=0 \tag{1}$$

$$\frac{\partial(\rho_{nf}u_iu_j)}{\partial x_i}=-\frac{\partial p}{\partial x_i}+\frac{\partial}{\partial x_j}\left[\mu_{nf}\left(\frac{\partial u_i}{\partial x_j}+\frac{\partial u_j}{\partial x_i}\right)\right] \tag{2}$$

$$\frac{\partial(u_j\theta)}{\partial x_i}=\frac{\partial}{\partial x_j}\left[\alpha_{nf}\frac{\partial\theta}{\partial x_j}\right] \tag{3}$$

The density, the effective thermal conductivity and the specific heat capacity of the nanofluid are calculated using the following equations respectively:

$$\rho_{nf}=(1-\varphi)\rho_f+\varphi\rho_s \tag{4}$$

$$\alpha_{nf}=\frac{k_{nf}}{(\rho C_p)_{nf}} \tag{5}$$

$$(\rho C_p)_{nf}=(1-\varphi)(\rho C_p)_f+\varphi(\rho C_p)_s \tag{6}$$

The viscosity of the nanofluid is represented by Einstein's equation [25]:

$$\mu_{nf}=\mu_f(1+2.5\varphi) \tag{7}$$

The thermal conductivity of the nanofluid (k_{nf}) is determined by the following relationship [26]:

$$\frac{k_{nf}}{k_f}=\frac{(k_s+2k_f)-2\varphi(k_f-k_s)}{(k_s+2k_f)+\varphi(k_f-k_s)} \tag{8}$$

In the preceding equations, φ, k_f, and k_s represent, respectively, the volume fraction of nanoparticles, the thermal conductivity of the base fluid, and the thermal conductivity of the solid nanoparticles.

The boundary conditions for the considered problem are expressed as follow:

- A constant velocity is applied at the inlet port and the gradients of all variables in the x- direction are set to zero at the exit port.
- No slip boundary conditions are considered over all the solid walls.

- The temperature of the heated ribs is higher than the inlet fluid temperature.

By using the following dimensionless variables:

$$X = \frac{x}{H},\quad Y = \frac{y}{H},\ P = \frac{p}{\rho_{nf} u_{in}^2}\ ,\ U = \frac{u}{u_{in}},\quad V = \frac{v}{u_{in}},\ T = \frac{\theta - \theta_{in}}{\theta_h - \theta_{in}}\ ,$$

the governing equations are then written in the dimensionless form:

$$\frac{\partial U}{\partial X} + \frac{\partial V}{\partial Y} = 0 \tag{9}$$

$$U\frac{\partial U}{\partial X} + V\frac{\partial U}{\partial Y} = -\frac{\partial P}{\partial X} + \frac{1}{Re}\frac{\mu_{nf}}{\rho_{nf}}\frac{\rho_f}{\mu_f}\left[\frac{\partial^2 U}{\partial X^2} + \frac{\partial^2 U}{\partial Y^2}\right] \tag{10}$$

$$U\frac{\partial V}{\partial X} + V\frac{\partial V}{\partial Y} = -\frac{\partial P}{\partial Y} + \frac{1}{Re}\frac{\mu_{nf}}{\rho_{nf}}\frac{\rho_f}{\mu_f}\left[\frac{\partial^2 V}{\partial X^2} + \frac{\partial^2 V}{\partial Y^2}\right] \tag{11}$$

$$U\frac{\partial T}{\partial X} + V\frac{\partial T}{\partial Y} = \frac{1}{Re.Pr}\frac{\alpha_{nf}}{\alpha_f}\left[\frac{\partial^2 T}{\partial X^2} + \frac{\partial^2 T}{\partial Y^2}\right] \tag{12}$$

4. Numerical Procedure

The dimensionless equations (9)-(12) are discretized using the finite volume approach, and the computational fluid dynamics (CFD) software FLUENT 16.0 is used to solve the nonlinear equation system iteratively. Velocity components are evaluated using a staggered grid, whereas scalar variables are calculated using a non-staggered grid. The resolution of pressure-velocity coupled equations is achieved by utilizing the SIMPLE algorithm [27]. We have set convergence criteria of 10^{-6} for the normalized residual of each equation.

4.1. Grid independence

We employed a grid-independent process to determine the suitable number of nodes, employing three meshes with varying grid sizes. The Reynolds number, calculated based on the inlet velocity and microchannel height, is defined as:

$$Re = \frac{\rho_{nf}.u_{in}.H}{\mu_{nf}} \tag{13}$$

For a Reynolds number (Re) of 100 and a nanoparticle volume fraction (φ) of 1%, the average error for the mean Nusselt number of the heated surface was below 0.40% between the first two meshes and less than 0.30% between the last two meshes, as indicated in Table 2. Therefore, the final mesh was selected based on its exceptional performance.

Table 2. Impact of the mesh size on the average Nusselt number of the heated surface.

Mesh size	Average Nusselt number	Relative deviation %
320x32	5.215	-
400x40	5.235	0.38
500x50	5.250	0.28

4.2. Code validation

To verify the accuracy of our mathematical model and numerical simulations, we have compared our results with those reported by Akbari et al. [4] and Aminossadati et al. [28] concerning laminar heat transfer in a smooth microchannel. The investigation explored Reynolds numbers of 10 and 100, considering various volume fractions (φ = 0.02, 0.03, and 0.04). The core section of the microchannel is subjected to a constant heat flux of 25000 W/m², while the remaining portions of the microchannel are thermally insulated from all directions, as depicted in Figure 2.

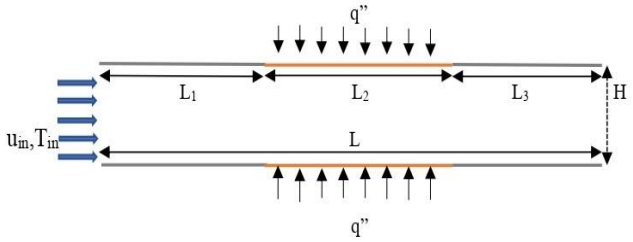

Figure 2. Configuration of Akbari et al. [4]

The average Nusselt number calculated for the heated portion of the microchannel showed significant consistency with the findings of the research cited ([4] and [28]), as depicted in Figure 3.

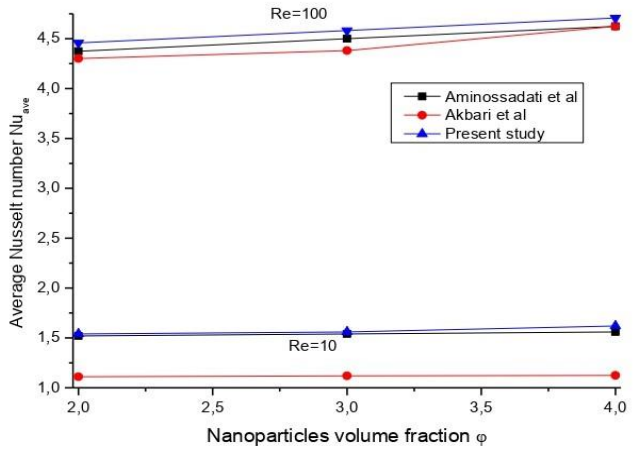

Figure 3. The validation of the mean Nusselt numbers for a smooth microchannel.

5. Results and Discussions

In this study, we performed numerical simulations of laminar mixed convection using Cu/Water nanofluid within a microchannel. The Reynolds numbers considered in the investigation span from Re = 20 to Re = 200. The research explores the influence of nanoparticles on the heat transfer rate by adjusting the nanoparticle fraction within the range of 1% to 8% (refer to Table 3). Furthermore, the investigation evaluates the impact of rib height at three specified values: e = 20 μm, e = 30 μm, and e = 40 μm.

Table 3. Thermophysical properties of nanofluid for different volume fractions.

	φ	φ = 2%	φ = 4%	φ = 8%
Cp_{nf} ($J.Kg^{-1}K^{-1}$)	3	3592.54	3147.71	2517.61
ρ_{nf} ($Kg.m^{-3}$)	1	1155.82	1314.54	1631.97
k_{nf} ($W.m^{-1}.K^{-1}$)	0.	0.650	0.689	0.772
μ_{nf} ($kg.m^{-1}.s^{-1}$)x10^5	8	89.77	94.05	102.6
α_{nf} ($m.s^{-2}$)x10^7	1.	1.57	1.66	1.88

Figure 4 illustrates the distribution of the local Nusselt number along the indentation wall for three distinct rib heights, maintaining a constant nanoparticle volume fraction of 8%. A consistent pattern in the behavior of the local Nusselt number is evident across all rib heights. The introduction of ribs on the lower surface of the microchannel induces sudden fluctuations in the Nusselt number. With the growth of the Reynolds number, the fluid velocity increases, amplifying the magnitude of these variations.

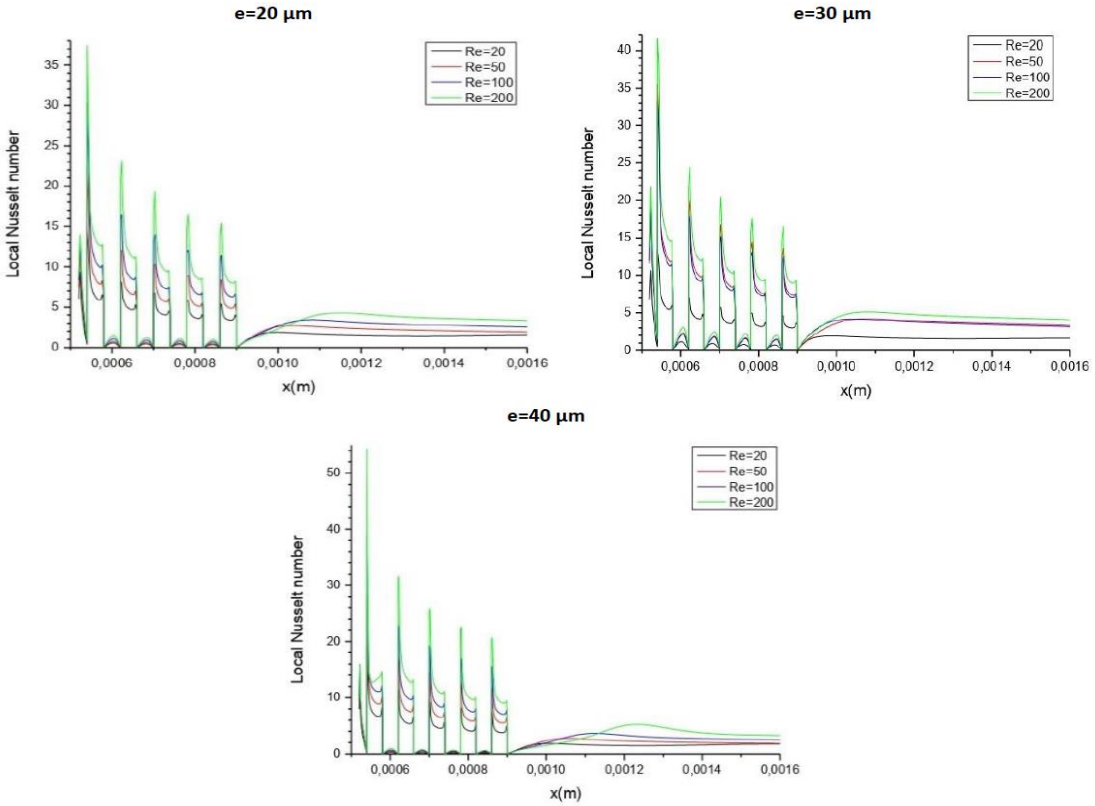

Figure 4. Local Nusselt variation for different rib's height

The initial rib consistently demonstrates the highest occurrence of sudden increases in the Nusselt number, irrespective of the rib's height. Subsequently, these abrupt changes gradually diminish as the fluid momentum decreases due to the interaction between the nanofluid and the ribs. A thickness of 40 µm consistently yields the highest Nusselt number.

In Figure 5, the correlation between the average Nusselt number and Reynolds number is depicted for a particle size of 30 µm and varying proportions of nanoparticles. The Nusselt number exhibits an approximately linear relationship with the Reynolds number. Increasing the Reynolds number induces

turbulent flows and enhances the convective heat transfer coefficient. On the contrary, when the volume percentage of solid nanoparticles is increased, only a minimal impact is observed on the heat transmission processes.

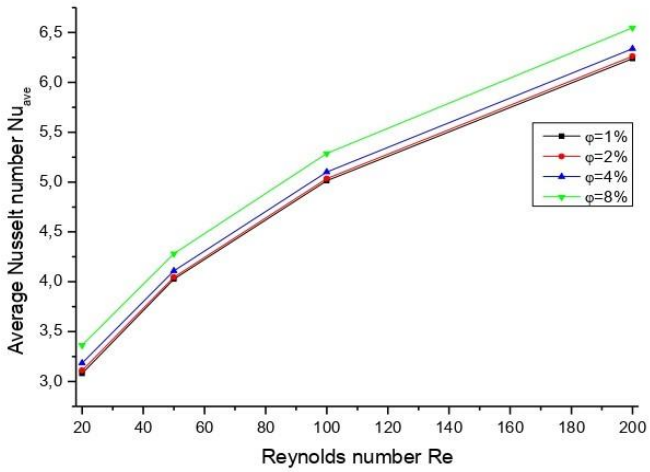

Figure 5. Average Nusselt number for different volume fractions.

Figure 6 illustrates the correlation between Reynolds numbers and the average Nusselt number for various rib heights. The enhancement of rib height contributes to an improvement in the heat transfer process, as the flow interacts with the ribs, causing alterations in hydrodynamic behavior and heat transmission. These changes are particularly prominent at high Reynolds numbers. At a Reynolds number of 200, a discrepancy of approximately 5.98% in the mean Nusselt number was observed between cases with gap sizes of 40 µm and 30 µm. However, a 0.87% discrepancy is noted between e = 30 µm and e = 20 µm for the same volume fraction.

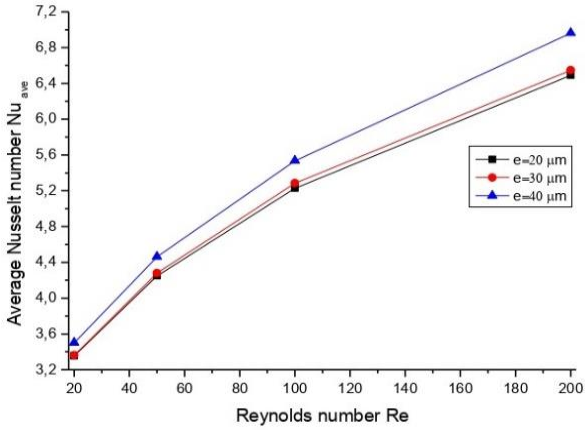

Figure 6. Average Nusselt number variation with Reynolds number for φ = 8 %.

The friction factor is defined as:

$$C_f = \frac{2.\tau_w}{\rho_{nf} u_{in}^2} \tag{14}$$

τ_w: denotes the wall shear stress (N/m^2).

Figure 7 demonstrates the variation in the local friction factor along the indented lower wall of the microchannel. The simulation findings confirm that raising the rib height results in an elevated friction factor. This occurrence is attributed to the heightened interaction between the ribbed surfaces of the ribs and the nanofluid.

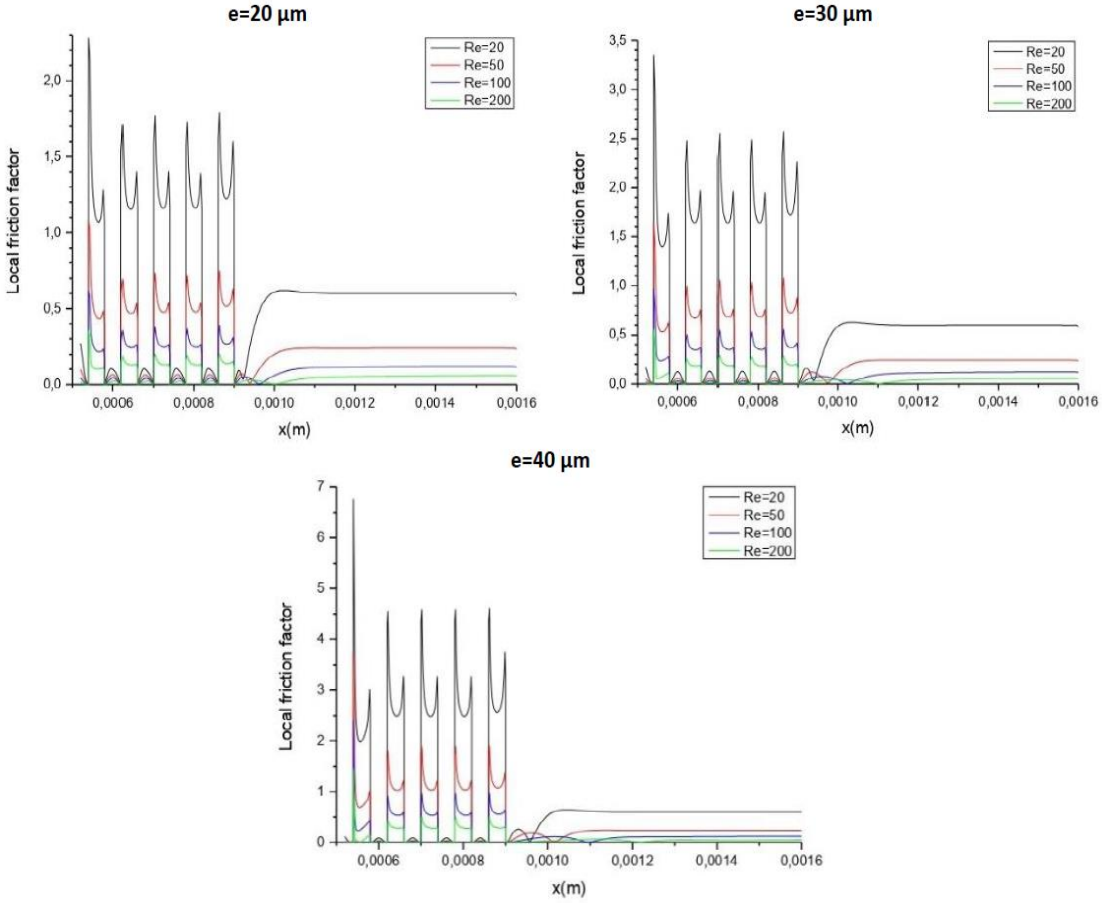

Figure 7. Local friction factor variation for different rib's height

In Figure 9(a), the graph depicts the association between the average friction factor and Reynolds number for a specific rib height (e = 30 µm) across varying nanoparticle volume fractions. The average friction factor exhibits a decline as Reynolds number increases, indicating more significant interaction between the flow and rib surfaces at lower Reynolds numbers compared to the interaction observed at higher Reynolds numbers. Furthermore, it can be inferred that the mean friction factor proportionally rises with the nanoparticle volume percentage. This effect is ascribed to the increase in dynamic viscosity resulting from the presence of suspended nanoparticles.

Shifting focus to Figure 9(b), the graph illustrates the correlation between the average friction factor and Reynolds numbers for different rib heights. It is noted that the friction factor decreases as Reynolds number increases for all rib heights. The elevation of rib height induces a decrease in pressure due to blockage, leading to an augmented shear rate and friction factor within the walls.

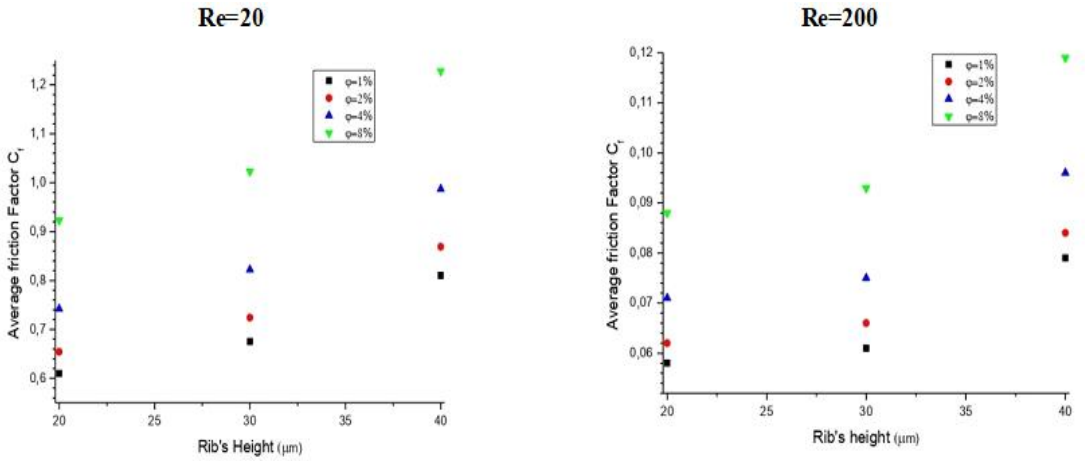

Figure 8. Average friction factor variation with volume fraction for Re = 20 and Re = 200

In Figure 9(a), the correlation between the average friction factor and Reynolds number is illustrated for a specific rib height (e = 30 µm) across different nanoparticle volume fractions. The average friction factor demonstrates a decrease with an increase in Reynolds number, suggesting a more substantial contact between the flow and rib surfaces at lower Reynolds numbers compared to the contact observed at higher Reynolds numbers. Additionally, it can be deduced that the mean friction factor proportionally increases with the nanoparticle volume percentage. This phenomenon is attributed to the augmentation of dynamic viscosity resulting from the presence of suspended nanoparticles.

Moving to Figure 9(b), the relationship between the average friction factor and Reynolds numbers is portrayed for various rib heights. It is observed that the friction factor diminishes as Reynolds number increases for all rib heights. The elevation of rib height leads to a reduction in pressure due to blockage, consequently causing an increase in shear rate and friction factor within the walls.

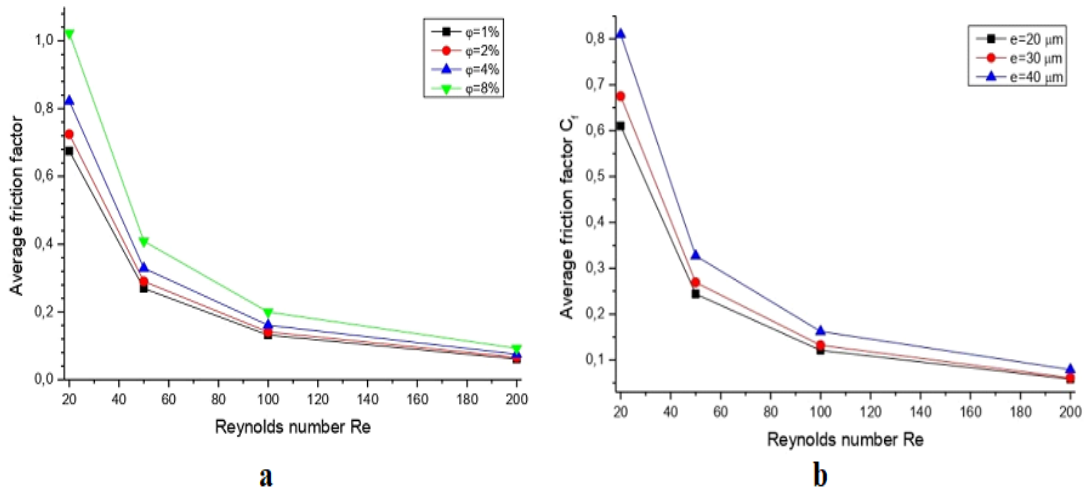

Figure 9. Average friction factor variation with Reynolds number: (a) For different volume fractions, (b) for different ribs height at φ = 1 %.

6. Conclusions

This study employed numerical analysis to investigate the influence of rib height on flow and heat transfer in a laminar nanofluid flow within a rectangular microchannel with indentations. The nanofluid, characterized by Newtonian and incompressible properties with constant features, experiences a temperature gradient of 5 °C between the inlet and the heated indentation wall. The research explores the effects of nanoparticles by varying the volume percentage from 1% to 8% across a Reynolds number range of Re = 20 to Re = 200.

The numerical results indicate that an increase in rib height (e = 20 μm, e = 30 μm, and e = 40 μm) enhances the interaction between the nanofluid and the indented wall, resulting in a higher friction factor. Notably, the average friction factor exhibits more pronounced effects at lower Reynolds numbers compared to higher Reynolds numbers. Additionally, heightened rib structures contribute to improved heat transfer coefficients, leading to higher Nusselt numbers. Regardless of rib height, an escalation in Reynolds number and nanoparticle volume fraction correlates with an increase in Nusselt number.

References

[1] Saidur, R., *et al*., A review on applications and challenges of nanofluids, *Ren. Sust. Energy Reviews,* 15 (2011), pp. 1646-1668.

[2] Khanafer, K., Vafai, K., A critical synthesis of thermophysical characteristics of nanofluids, *International Journal of Heat Mass Transfer,* 54 (2012), pp. 4410-4442.

[3] Tuckerman, D. B., Pease, R.F.W., High performance heat sinking for VLSI, *IEEE Electron Device Letters,* 2 (1981), 5, pp. 126-129.

[4] Akbari, O. A., *et al*., Impact of ribs on flow parameters and laminar heat transfer of water– aluminum oxide nanofluid with different nanoparticle volume fractions in a three-dimensional rectangular microchannel, *Advances in Mechanical Engineering,* 7 (2015), 11, pp. 1-11.

[5] Alipour, H., *et al*., Influence of T-semi attached rib on turbulent flow and heat transfer parameters of a silver-water nanofluid with different volume fractions in a three-dimensional trapezoidal microchannel, *Physica E*, 88 (2017), pp. 60-76.

[6] Esfahani, M.A, Toghraie, D., Experimental investigation for developing a new model for the thermal conductivity of Silica/Water-Ethylene glycol (40%–60%) nanofluid at different temperatures and solid volume fractions, *Journal of Molecular Liquids*, 232 (2017), pp. 105-112.

[7] Aghanajafi, A., *et al*., Numerical simulation of laminar forced convection of Water-CuO nanofluid inside a triangular duct, *Physica E*, 85 (2017), pp. 103-108.

[8] Arabpour, A., *et al*., The study of heat transfer and laminar flow of kerosene/multi-walled carbon nanotubes (MWCNTs) nanofluid in the microchannel heat sink with slip boundary condition, *journal of Thermal Analysis Calorimetry*, 131 (2018), pp. 1553-1566.

[9] Hadi Najafabadi, H., Keshavarz Moraveji, M., CFD investigation of local properties of Al_2O_3/water nanofluid in a converging microchannel under imposed pressure difference, *Advanced Powder Technology,* 28 (2017), 3, pp. 763-774.

[10] Khodabandeh, E., *et al*., Numerical investigation of thermal performance augmentation of nanofluid flow in microchannel heat sinks by using of novel nozzle structure: sinusoidal cavities and rectangular ribs, *Journal of the Brazilian Society of Mech. Sci. and Eng,* 41 (2019), 443.

[11] Mir, S., *et al*., A comprehensive study of two-phase flow and heat transfer of water/Ag nanofluid in an elliptical curved minichannel, *Chinese Journal of Chemical Engineering*, 28 (2020), pp. 383-402.
[12] Gholami, M. R., *et al*., The effect of rib shape on the behavior of laminar flow of oil/MWCNT nanofluid in a rectangular microchannel, *Journal of Thermal Analysis Calorimetry*, 137 (2018), pp. 1611-1628.
[13] Afrouzi, H. H., *et al*., Thermo-hydraulic characteristics investigation of nanofluid heat transfer in a microchannel with super hydrophobic surfaces under non-uniform magnetic field using Incompressible Preconditioned Lattice Boltzmann Method, *Phys. A*, 553 (2020), 124669.
[14] Dehghani, M. S., *et al*., Mixed-convection nanofluid flow through a grooved channel with internal heat generating solid cylinders in the presence of an applied magnetic field, *Heat Transfer Research*, 50 (2019), 3, pp. 287-309.
[15] Arasteh, H., *et al*., Optimal arrangements of a heat sink partially filled with multilayered porous media employing hybrid nanofluid, *J. Thermal Analysis Calorimetry*, 137 (2019), pp. 1045-1058.
[16] Nojoomizadeh, M., *et al*., Investigation of permeability effect on slip velocity and temperature jump boundary conditions for FMWNT/Water nanofluid flow and heat transfer inside a microchannel filled by a porous media, *Physica E*, 97 (2018), pp. 226-238.
[17] Nazari, S., Toghraie, D., Numerical simulation of heat transfer and fluid flow of Water-CuO Nanofluid in a sinusoidal channel with a porous medium, *Physica E*, 87 (2017), pp. 134-140.
[18] Rahmati, A. R., *et al*., Simultaneous investigations the effects of non-Newtonian nanofluid flow in different volume fractions of solid nanoparticles with slip and no-slip boundary conditions, *Thermal Science and Engineering Progress*, 5 (2018), pp. 263-277.
[19] Barnoon, P., Toghraie, D., Numerical investigation of laminar flow and heat transfer of non-Newtonian nanofluid within a porous medium, *Powder Technology*, 325 (2018), pp. 78-91.
[20] Syah, R., *et al*., Numerical investigation of nanofluid flow using CFD and fuzzy-based particle swarm optimization, *Scientific Reports*, 11 (2021), 20973.
[21] Temiloluwa, O. S., *et al*., Experimental investigation of natural convection Al_2O_3-MWCNT/water hybrid nanofluids inside a square cavity, *Experimental Heat Transfer*, (2022).
[22] Moghadasi, H., *et al*., A computational fluid dynamics study of laminar forced convection improvement of a non-Newtonian hybrid nanofluid within an annular pipe in porous media, *Energies*, 15 (2022), 8207.
[23] Gravndyan, Q., *et al*., The effect of aspect ratios of rib on the heat transfer and laminar water/ TiO_2 nanofluid flow in a two-dimensional rectangular microchannel, *Journal of Molecular Liquids*, 236 (2017), pp. 254-265.
[24] Incropera, F.P., De Witt, D.P., *Introduction to Heat Transfer*, 4th edition, Wiley., New York, USA. 2002.
[25] Drew, D.A., Passman, S.L., *Theory of multicomponent fluids*, Springer-Verlag., New York, USA, 1999.
[26] Maxwell, J. C., *A Treatise on Electricity and Magnetism*, Unabridged., Dover, USA, 1954.
[27] Patankar, S.V., *Numerical Heat Transfer and Fluid Flow*, Mac Graw Hill., New York, USA, 1980.
[28] Aminossadati, S. M., *et al*., Effects of magnetic field on nanofluid forced convection in a partially heated microchannel, *International Journal of Nonlinear Mechanics*, 46 (2011), pp. 1373-1382.

Submitted: 06.02.2024
Revised: 04.03.2024
Accepted: 15.04.2024